

**LaJolla**  
**INSTITUTE**

CENTER FOR STUDIES OF NONLINEAR DYNAMICS  
7855 FAY AVENUE, SUITE 320  
LA JOLLA, CALIFORNIA 92037

LJI-87-P-467

(4) (12)

AD-A203 604

ITC FILE COPY

**Imaging of Ocean Waves by SAR**

Contract N00014-87-C-0687

DTIC  
ELECTE  
JAN 24 1989  
S D

R.L. Schult  
F.S. Henyey  
J.A. Wright

**Center for Studies of Nonlinear Dynamics**

**La Jolla Institute**

**7855 Fay Avenue, Suite 320**

**La Jolla, California 92037**

DISTRIBUTION STATEMENT A

Approved for public release  
Distribution Unlimited

**LJI-87-P-467**

## Imaging of Ocean Waves by SAR

**R.L. Schult**

**F.S. Henyey**

**J.A. Wright**

**Center for Studies of Nonlinear Dynamics**

**La Jolla Institute**

**7855 Fay Avenue, Suite 320**

**La Jolla, California 92037**

Accession # 100  
NTIS CRASH  
DTIC TAB  
Unannounced  
Justification  
By per ltr  
Date  
A-1



## Abstract

We present a model for Synthetic Aperture Radar imaging of the ocean surface. In constructing the model we attempt to avoid making assumptions about the relative importance of various imaging mechanisms. We apply the model to three issues, the focus setting, the asymmetry in the images obtained with opposite airplane flight directions, and the azimuthal image shift of features on range directed waves. We show that the focus setting depends on a combination of the velocity of the pattern being imaged and on the velocity of the Bragg scatterers. The focus setting does not depend significantly on the imaging mechanism, that is velocity bunching, modulation of Bragg waves, and so on. Comparisons of our model predictions are made with the TOWARD results. We obtain a simple analytic prediction of the complete curve of the observed energy in swell versus the focus setting. We predict that the maximum of this curve occurs at one-half of the phase speed of the swell for azimuthally traveling swell and we provide a simple explanation of this result. We estimate the asymmetry in the visibility of the swell obtained by flying with or against the long waves. The asymmetry arises from competition between velocity bunching and hydrodynamic modulations.

In a companion paper we present a detailed analysis of the TOWARD data.

## Imaging of Ocean Waves by SAR

### 1. Introduction

Synthetic Aperture Radar images of long-wavelength features on the ocean surface are obtainable from both airplanes and satellites. Some of the mechanisms which contribute to the image formation are well established. On the other hand, there is controversy about the details of the effects of the time dependence of the ocean surface on the imaging process. In this article we present a model which attempts to avoid making assumptions about the relative importance of various aspects of the process so that the model can resolve some of the controversy. The model is applied to three issues, the focus setting, the asymmetry in the images obtained with opposite airplane directions, and the azimuthal image shift of features on range-directed waves. Comparison is made with other models which have been presented in the literature to see where the underlying physical assumptions have led to divergent points of view.

The imaging of ocean features via SAR differs from that of land imaging in a number of respects. SAR relies on the temporal variation of phase information in order to resolve the azimuthal dimension. Because the ocean surface is in non-uniform motion the resulting phase changes disturb the image. The actual scattering is often dominated by Bragg scattering, and if, as often happens the Bragg waves lose phase coherence in a time less than the look time, then the azimuthal resolution is degraded. The motion of the Bragg waves due to their own phase velocity and to advection by larger waves leads to an incorrect location on the image. The fact that the advecting velocities vary from one part of the ocean to another leads to a smearing of the image.

Another problem is involved when some rapidly moving feature of the ocean is imaged. The simplest example, studied in TOWARD, occurs when a nearly monochromatic swell is present which is traveling in the azimuthal direction. The phase velocity of the swell is on the order of 10-20 meters per second while advecting velocities of the scatterers due to orbital motion are less than one m/sec. The intensity of scattering from different regions of the ocean surface as observed in the output of the SAR processor is correlated with the phase of the swell. As the swell moves the magnitude of scattering from a small scattering region has a dominant space-time dependence which is a function of  $X - v_\phi t$  where  $X$  is the azimuthal coordinate,  $v_\phi$  is the phase velocity of the swell and  $t$  is time. This also would be true of a solid body, moving with  $v_\phi$ . However, the phase of the radar return from a small patch of ocean does not have this dependence, whereas for a solid body it would. The velocities important for phase changes are the advecting velocities and the phase velocities of the Bragg waves. In order to understand

SAR imaging of the ocean it is important to understand this difference in the phase and amplitude behavior between solid patterns and ocean patterns. The origin of one of the controversies mentioned above is based in how to properly treat the various velocities.

Our most significant and surprising result is for the optimal focus setting for azimuthally directed long waves. For a stationary scene, standard SAR theory shows that the optimum focus setting is proportional to the square of the velocity of the airplane (or satellite). For a moving, but solid, scene, clearly one should use the square of the relative velocity,  $v_a - v_x$ , between the airplane (moving in the x direction at velocity  $v_a$ ) and the scene (moving at azimuthal velocity  $v_x$ ). For ocean waves, however, there are several relevant azimuthal velocities associated with the scene. These are the phase velocity,  $v_\phi$ , of the long waves being imaged, the phase velocity,  $u_\phi$ , of the shorter Bragg scattering waves responsible for the radar reflection, and the current velocity,  $u_c$ , (which could be the orbital velocity of the long wave) which advects the short waves. One school of thought [Jain (1978, 1981)] predicts that  $(v_a - v_\phi)^2$  should be used for the focus setting, while another [Alpers and Rufenach (1979)] predicts that  $(v_a - u_c)^2$  should be used. Jain and Shemdin (1983) have presented data indicating evidence for a velocity larger than  $u_c$ . Harger [1986] considers the case of an ensemble of Bragg waves entirely in the range direction riding on a long wave, for which the correct focus setting is also  $(v_a - v_\phi)^2$ . Our model makes the rather surprising prediction that both the pattern velocity and the velocity of the Bragg scatterers are important but that they contribute to different aspects of the SAR imaging process. The correct optimum focus setting involves  $(v_a - v_\phi)(v_a - u_c) \approx [v_a - (v_\phi + u_c)/2]^2$ . Since constructing our model we have discovered that Ivanov (1982, 1983), Rotherham (1983) and Ouchi (1983b) have also predicted  $(v_a - v_\phi/2)^2$ . Our result differs from theirs only in that it is explicitly independent of which reference frame is used for measuring velocities. We also show that this result is implicitly contained in the method of simulation proposed by Plant and Keller (1983).

We predict an asymmetry in the image contrast obtained flying with or against the long waves due to the interaction of the velocity bunching mechanism of imaging and the hydrodynamic and tilt-modulation mechanisms. Using preliminary data from the Univ. of Kansas component [Moore, et al. (1986)] of the TOWARD experiment [Shemdin, et al. (1986)] we make estimates of the sign of this asymmetry.

We also make comments on some aspects of imaging when the long waves are traveling in the range direction. These aspects might be tested using long narrow slicks on range directed waves.

Our model is presented in Section 2 for the general case. In Section 3 we treat the special case of a single long wave pattern. Section 4 compares other models. Section 5 deals with image contrast while flying with or against the wave propagation direction and Section 6 contains comments about various other long wave orientations and the more realistic case of the presence of several long waves. Appendices, A, B, C and D discuss simplified models to illustrate the imaging mechanisms. Appendix C in particular discusses the model discussed by Harger [1985], and shows that although his analysis is correct, his model treats an exceptional case. Appendix D is a discussion of decorrelation times for Bragg waves and the corresponding image degradation. In a companion paper, "Comparison of Computed SAR Focus-Setting Curves with Model predictions," DeWitt et al., [1988] we present a detailed comparison of our model with the TOWARD experiment.

## 2. The Model

### A. General Assumptions

Our model is based on a standard application of the SAR theory to the ocean surface which is thought of as having two scales. The short waves ( $\lambda \approx 0.25\text{m}$  for L-band) are responsible for the backscattering of the radar waves by way of the Bragg scattering mechanism. The long waves ( $\lambda \approx 140\text{m}$  for the TOWARD experiment) are responsible for modulating the short waves in such a way as to produce an image of the long waves. Long waves of intermediate size ( $\lambda \approx 20\text{m}$ ) may also play an important role in limiting the coherence time of the short waves through differential advection, for example, and thus may influence the effective length of the synthesized aperture. We treat the coherence time phenomenologically, but have also estimated it in Appendix D.

One modification to the standard SAR integrals which we have found helpful for analytic work is the use of a Gaussian shape for the resolution functions and time filter functions instead of the square windows usually employed. This change should not have a significant effect on the qualitative results, although it does introduce an ambiguity in comparing values of parameters such as the width of the time filter function to those used in specific experiments.

A central assumption of our model is that speckle in the image is relatively unimportant. We calculate the intensity of the image, which is the image amplitude squared. We assume that the product  $a^* a$  of the radar scattering amplitude and its conjugate (at the same time but different positions) can be replaced by its average over an ensemble of possible Bragg waves. (A model for the product at non-equal times is introduced in the next section in terms of that at equal times.) The Fourier transform of this product with respect to the position difference gives a spectrum, which depends on wave number  $K$ ,

average position  $\vec{R}$ , and time  $T$ . The  $\vec{R}$  and  $T$  dependence reflect modulation by long waves. We assume this spectrum to be a smooth function of all three variables. Although we assume the spectrum to be smooth in  $K$ , we do not assume, at present, anything else about the  $K$  dependence and how it is modulated by the long wave, except that if only one long wave (with phase velocity  $v_\phi$ ) is present, the modulation is a periodic function of  $\vec{R} - \vec{v}_\phi T$ .

### B. Detailed Formulae

A model for the imaging of the ocean surface by the SAR process must deal with the reflectivity of the surface to radar waves and with the effect that the time dependence of the ocean has on the SAR processing. The reflectivity is generally believed to be adequately described by a two-scale model which says that the locally reradiated electromagnetic field is proportional to the incident field times an obliquity factor such as the cosine of the angle of incidence,  $\delta$ , to the locally smooth (on the scale of the radar wavelength) surface. For an ocean surface described by the time-dependent height,  $h(x, y, t)$ , of the water relative to a horizontal  $x, y$  plane, the two scale model is

$$h(x, y, t) = A(x, y, t) + a(x, y, t) \quad (1)$$

where  $A$  and  $a$  are the contributions to the wave height from long wavelength and short wavelengths respectively. The locally smooth surface is then defined by  $A(x, y, t)$  and the angle of incidence varies with position and time as

$$\cos \delta d(\text{area}) = \left[ \cos \delta_0 + \frac{\partial A}{\partial y} \sin \delta_0 \right] dx dy \quad (2)$$

for a beam directed in the  $y - z$  plane at angle  $\delta_0$  from vertical. The factor  $\partial A / \partial y$  provides a tilt modulation of the reflectivity and is one of the ways in which the ocean might be imaged. For vertical radar polarizations there are important corrections to this simple obliquity factor, but it is probably adequate for the horizontal radar polarization and some aspects of the modeling do not depend on the exact form used.

The other ways in which the radar return is influenced by the ocean surface are through the phase difference induced by the varying path lengths to different parts of the surface. The geometry of SAR is illustrated in Figure 1 where the distance,  $R$ , from the airplane (or other radar platform) located at  $(x, y, z) = (v_a t, 0, h_0)$  to the ocean surface located at  $(x, y, z) = [x, y, h(x, y, t)]$  is given by

$$\begin{aligned} R &= \left\{ y^2 + [h_0 - h(x, y, t)]^2 + (x - v_a t)^2 \right\}^{1/2} \\ &\equiv R_0 + (y - y_0) \sin \delta_0 - h(x, y, t) \cos \delta_0 + \frac{(x - v_a t)^2}{2R_0} \end{aligned} \quad (3)$$

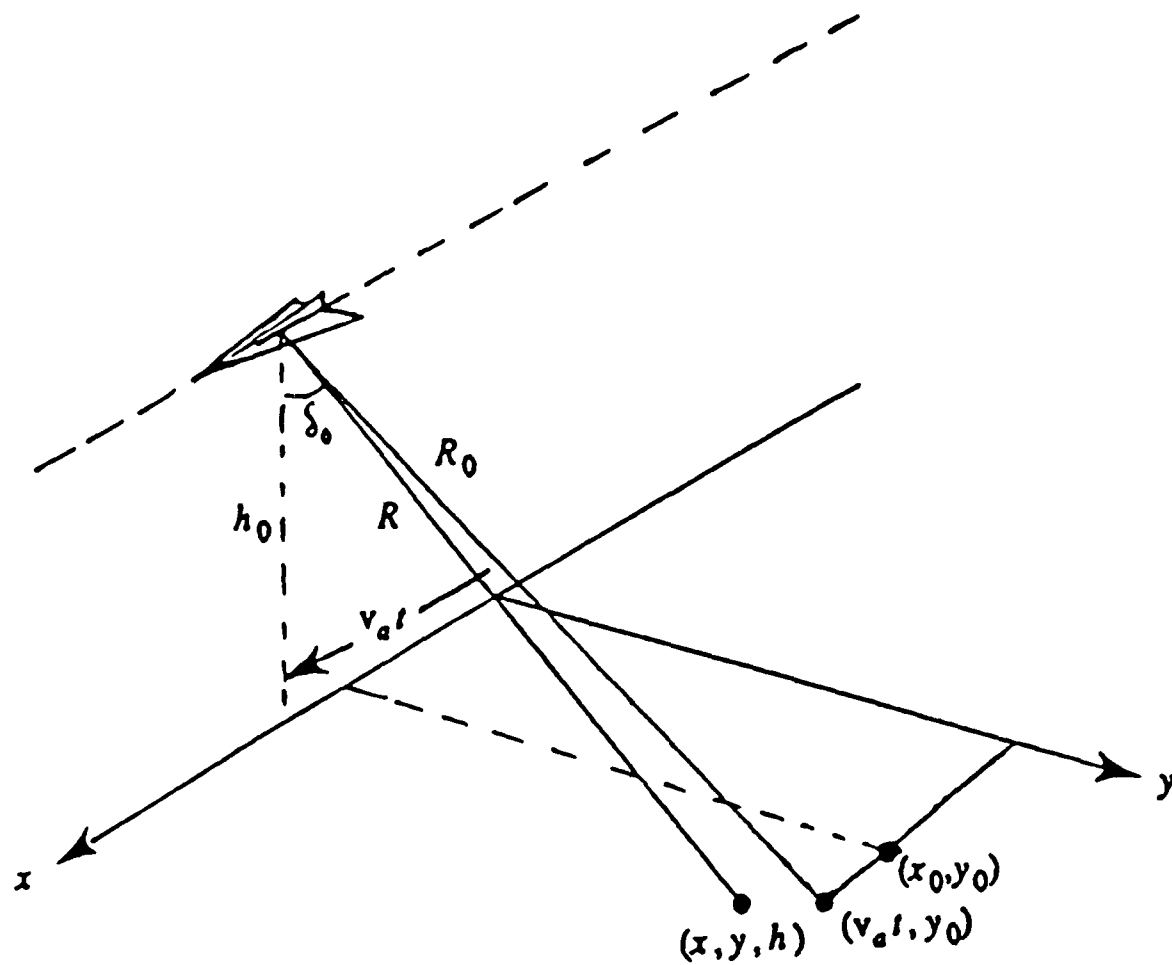


Figure 1. Geometry of SAR.

for points labeled by  $(x, y)$  near the point  $(x_0, y_0)$ . The radar pulse returns to the platform with a phase delay which is given by

$$\phi = k_r (2R) = (2\pi/\lambda) 2R \quad (4)$$

where  $\lambda$  is the radar wavelength. The modulation of this phase by the surface height  $h(x, y, t)$  provides the other mechanisms for imaging the surface.

In the two-scale model the part of the phase factor,  $e^{i\phi}$ , coming from the short waves can be expanded as a power series in  $k_r a$ , i.e.,

$$\exp[-2ik_r \cos \delta_0 a(x, y, t)] \approx 1 - 2ik_r \cos \delta_0 a(x, y, t) \quad (5)$$

The signal received at the platform and assigned to the nominal range distance  $y_0$  is an integral of the field over the  $x, y$  resolution of the radar beam

$$\begin{aligned} sig(y_0, t) = \iint dx dy Res_y(y - y_0) Res_x(x - v_a t) e^{2ik_r R_0} \exp[2ik_r \sin \delta_0 (y - y_0)] \\ \exp[-2ik_r \cos \delta_0 A(x, y, t)] \exp\left[ik_r \frac{(x - v_a t)^2}{R_0}\right] F(x, y, t) \quad (6) \end{aligned}$$

where

$$F(x, y, t) = [1 - 2ik_r \cos \delta_0 a(x, y, t)] \left[ \cos \delta_0 + \frac{\partial A}{\partial y} \sin \delta_0 \right] \quad (7)$$

This expression for the single pulse radar return depends upon the range resolution function  $Res_y(y - y_0)$ , the width of which may be determined by the duration of the pulse or it may be narrowed by the use of the "chirping" technique. In either case it is normally many radar wavelengths ( $\sim 45$  for TOWARD) wide. The azimuthal resolution function  $Res_x(x - v_a t)$  is determined by the antenna size and for SAR is typically quite wide (several thousand radar wavelengths). The integration over  $x$  and  $y$  essentially picks out the part of the factor  $F(x, y, t)$  which has the wave number  $k_y \equiv 2k_r \sin \delta_0$  and  $k_x \equiv 0$  corresponding to Bragg scattering from the little waves. These Bragg waves, however, are modulated by the large waves through both the obliquity factor and the heaving factor

$$\exp[-2ik_r \cos \delta_0 A(x, y, t)] \quad (8)$$

as well as by the hydrodynamic interaction of the big waves with the little waves. The hydrodynamics enter as variations in the size of the amplitude  $a(x, y, t)$  of the Bragg waves in different regions of the ocean surface.

The time dependence of the surface height  $h = A + a$  becomes important when the single pulse radar returns of (6) for various times are combined by the SAR processor to improve the azimuthal resolution. The idea is to use the quadratic time dependence of

the phase as a "lens" to focus on particular values of  $x$ . The procedure is to multiply (6) by

$$\exp \left[ \frac{-ik_r (x_0 - v_a t)^2}{R_0} (1 - v_f/v_a)^2 \right] \text{Res}_t (x_0 - v_a t) \quad (9)$$

and sum over a large number of pulses (labeled by  $t$ ) for each desired value of  $x_0$ . The factor  $(1 - v_f/v_a)^2$  is a focus setting correction to remove any defocusing caused by quadratic time dependent phases generated by the time dependence of the ocean surface. The phase term involving  $x_0$  steers the focusing onto different points of stationary phase in the  $t$  sum. When the radar pulse repetition rate is large the sum over the pulses can be replaced by an integral with some resolution window  $\text{Res}_t (x_0 - v_a t)$  which determines how many pulses are used to reconstruct the final image to be associated with the point  $(x_0, y_0)$ . The resulting triple integral over  $x, y, t$  would be a large but finite problem, if  $A(x, y, t)$  and  $a(x, y, t)$  were known, but since they are not, they must be modeled.

For special time dependences the  $t$  integral can be done. These special cases usually involve constant velocity or constant acceleration of a patch of the ocean. For example, if  $A$  and  $a$  are functions of  $x - v_x t$  and  $y$  only, then a change of variable from  $x$  to  $z = x - v_x t$  leaves all the time dependence of (6) in the factor

$$\text{Res}_x [z - (v_a - v_x) t] \exp \left\{ ik_r \frac{[z - (v_a - v_x) t]^2}{R_0} \right\} \quad (10)$$

so it is readily seen that the proper focus is

$$v_f = v_x \quad (11)$$

If  $A$  and  $a$  are functions of  $x$  and  $y - v_y t$  only, a different change of variable from  $y$  to  $z' = y - v_y t$  is equivalent to changing  $x_0$  to  $x_0 + (R_0/v_a) v_y \sin \delta_0$  producing a (large) velocity shift in the  $x$ -direction due to motion of the scattering object in the radial direction, and no focus correction. (Combinations of the two effects can occur with no complications.) The ocean surface, however, does not have a single velocity and the phase velocity  $v_0$  appropriate for the large wave,  $A$ , is not the same as the velocities characteristic of the small wave,  $a$ . A single change of variables is not sufficient.

Our model attempts to get around the problem of several velocities by treating the little waves (which may have short correlation times) statistically. This is accomplished by squaring the triple integral for the processed image field and using instead of the variables  $x, y, t, x', y', t'$  the average and difference variables

$$\begin{aligned} X &= \frac{x+x'}{2}, \quad \delta x = x - x' \\ Y &= \frac{y+y'}{2}, \quad \delta y = y - y' \\ T &= \frac{t+t'}{2}, \quad \delta t = t - t'. \end{aligned} \quad (12)$$

It is extremely convenient to use Gaussian functions for the resolution functions in analytical calculations even though the actual apparatus may not use a Gaussian window. The final details may not be exactly correct but the qualitative features should be. The advantage is that  $Res_x(x) Res_x(x') = Res_x(\sqrt{2}X) Res_x(\delta x/\sqrt{2})$  and that various integrals can be done analytically.

We obtain

$$\begin{aligned} \text{Image} &= \left| \text{Sig}(x_0, y_0) \right|^2 = \left| \int dx dy dt Res_y(y - y_0) Res_x(x - v_a t) Res_t(x_0 - v_a t) \right. \\ &\quad \exp[2ik_r \sin \delta_0 (y - y_0)] \exp[-2ik_r \cos \delta_0 A(x, y, t)] \\ &\quad \left. F(x, y, t) \exp \left\{ \frac{ik_r}{R_0} \left[ (x - v_a t)^2 - (x_0 - v_a t)^2 (1 - v_f/v_a)^2 \right] \right\} \right|^2 \\ &= \int dX dY dT d\delta x d\delta y d\delta t \left\{ Res_y[\sqrt{2}(Y - y_0)] Res_y(\delta y/\sqrt{2}) \right. \\ &\quad Res_x[\sqrt{2}(X - v_a T)] Res_x\left[\frac{\delta x - v_a \delta t}{\sqrt{2}}\right] \\ &\quad Res_t[\sqrt{2}(x_0 - v_a T)] Res_t\left[\frac{\delta t v_a}{\sqrt{2}}\right] \\ &\quad \exp(2ik_r \sin \delta_0 \delta y) \exp\{2ik_r \cos \delta_0 [A(x', y', t') - A(x, y, t)]\} \\ &\quad \exp \left\{ \frac{2ik_r}{R_0} \left[ (X - v_a T)(\delta x - v_a \delta t) + x_0 v_a \delta t (1 - v_f/v_a)^2 - (v_a - v_f)^2 T \delta t \right] \right\} \\ &\quad \left. F(x, y, t) F^*(x', y', t') \right\}. \end{aligned} \quad (13)$$

Anticipating that the time integrals produce a narrow resolution in the  $x$  integration ( $\sim 11\text{m}$  for TOWARD) we can use the fact that the long wave amplitudes are slowly varying on the resolution scale and expand about the average coordinates  $X, Y, T$  obtaining

$$A(x', y', t') - A(x, y, t) = -\frac{\partial A}{\partial T}(X, Y, T) \delta t - \vec{\nabla} A(X, Y, T) \cdot \delta \vec{r} \quad (14)$$

plus cubic terms. The rapidly varying factor  $F$  can be analyzed as

$$F(x, y, t) F^*(x', y', t') = a(x, y, t) a^*(x', y', t') G(x, y, t, x', y', t') \quad (15)$$

where  $G$  is a slowly varying factor describing changes in the obliquity factor due to tilting of the surface by the long waves.

The small waves are probably correlated over moderately short distances and times, and are modulated by the big waves over longer times. First consider the equal-time product

$$a(x, y, T) a^*(x', y', T) = \int d^2 K e^{i\vec{K} \cdot (\vec{r} - \vec{r}')} Sp\left[\frac{\vec{r} + \vec{r}'}{2}, T, \vec{K}\right] \quad (16)$$

In the present treatment we wish to ignore speckle and hence replace  $aa^*$  by an ensemble average. In this case  $Sp(\vec{R}, T, \vec{K})$  is the local spectrum of the little waves and is assumed to be a smooth function of its arguments.

For the case of slowly varying  $Sp(\vec{R}, T, \vec{K})$  we can treat the non-equal time case by neglecting momentarily the  $\vec{R}$  dependence in which case the  $e^{i\vec{K} \cdot \vec{r}}$  factor in (16) should go with a time dependence  $e^{-i\omega_K t}$  where

$$\omega_K = \pm (\sigma_K) + (\vec{u} \cdot \vec{K}) \quad (17)$$

are the frequencies of Bragg waves of wave number  $\vec{K}$  in the advecting current  $\vec{u}(\vec{R}, T)$  which is, of course, modulated by the long waves. The two sign choices correspond to the two directions of propagation for each  $\vec{K}$ . The intrinsic frequency  $\sigma_K$  may also be modulated by the long waves by changing the effective gravity felt by the little waves. For a more complete discussion of the interaction of short waves with long waves, see Henyey et al., 1988. Damping, wind, and modulation by intermediate size waves should lead to a decorrelation of these Bragg waves. We treat this phenomenologically through a function

$$D(t - t') = e^{-\frac{(t - t')^2}{4\tau_c^2}} \quad (18)$$

where  $\tau_c$  is a measure of the decorrelation time. Using (17) for both  $e^{i\vec{K} \cdot \vec{r}}$  and  $e^{-i\vec{K} \cdot \vec{r}'}$  leads to

$$a(x, y, t) a^*(x', y', t') = \int d^2 K e^{i\vec{K} \cdot (\vec{r} - \vec{r}')} e^{-i\omega_K(\vec{R}, T)(t - t')} Sp(\vec{R}, T, \vec{K}) D(t - t') \quad (19)$$

at least for small  $t - t'$ . The presence of a decorrelation time makes the expansions in the time difference,  $\delta t$ , [as in Eq. (14) for example] more justified than similar expansions in the average time variable,  $T$ , would be since  $T$  is limited only by the look time which may be longer than the decorrelation time. We will return to this point in Section 4.

Returning to our complete expression (13) for the final SAR image we see that the  $\delta x$  and  $\delta y$  integrals can be performed in this approximation as Fourier transforms of the Gaussian resolution functions  $Res_x$  and  $Res_y$  with arguments

$$-2k_r \cos \delta_0 \frac{\partial A}{\partial X} (\vec{R}, T) + 2k_r \left[ \frac{X - v_a T}{R_0} \right] + K_x$$

and

$$2k_r \sin \delta_0 - 2k_r \cos \delta_0 \frac{\partial A}{\partial Y} (\vec{R}, T) + K_y \quad (20)$$

respectively. For sufficiently wide resolution functions in  $\delta x$  and  $\delta y$  these Fourier transforms are essentially  $\delta$ -functions of their arguments. They tell us which Bragg waves are picked out by the SAR including the usual result

$$\vec{K} = (0, -2k_r \sin \delta_0) \quad (21)$$

plus the corrections due to  $\vec{\nabla} A$ , the tilting of the surface by the long waves, and also the small rotation of the beam as the airplane passes a particular portion of the ocean. Treating these as  $\delta$ -functions allows the  $d^2 K$  integrals to be done. The  $\delta t$  integral is now the Fourier transform

$$\tilde{R}_t(\omega) \equiv \int d\delta t Res_t \left[ \frac{v_a \delta t}{\sqrt{2}} \right] D(\delta t) e^{i\omega \delta t} \quad (22)$$

with argument

$$\begin{aligned} \omega \equiv & \pm \sigma_k + 2k_r \sin \delta_0 u_y - 2k_r \cos \delta_0 \vec{\nabla} A \cdot \vec{u} - 2k_r \cos \delta_0 \frac{\partial A}{\partial T} \\ & + \frac{2k_r}{R_0} v_a [x_0 (1 - 2v_f/v_a) - X + 2v_f T] + 2k_r u_x \frac{X - v_a T}{R_0} . \end{aligned} \quad (23)$$

The first four terms of  $\omega$  can be recognized as  $2k_r v_a / R_0$  times the usual velocity shift of  $x_0$ :

$$x_0 \rightarrow x_0 \left[ 1 - \frac{2v_f}{v_a} \right] + X_{sh} = x_0 \left[ 1 - \frac{2v_f}{v_a} \right] + \frac{R_0 \sin \delta_0}{v_a} \left[ u_y - \cot \delta_0 u_z \pm \frac{\sigma_k}{2k_r \sin \delta_0} \right] , \quad (24)$$

and we have dropped terms of order  $(v_f/v_a)^2$ . The last term in (23) is a time dependent velocity shift caused by the fact that in the presence of advection the frequency of the Bragg waves being sampled by the radar beam is different depending on whether the patch of ocean is slightly ahead or slightly behind the point directly beside the antenna. This term is usually omitted as being small but the  $R_0/v_a$  factor in the velocity shift gives it more significance than initially meets the eye.

Collecting the result of doing the  $\delta x, \delta y, \vec{K}$  and  $\delta t$  integrals leaves us with

$$\begin{aligned} \text{Image}(x_0, y_0) = \int dX dY dT \text{Res}_y[\sqrt{2}(Y - y_0)] \text{Res}_x[\sqrt{2}(X - v_a T)] \\ \text{Res}_t[\sqrt{2}(x_0 - v_a T)] Sp(\vec{R}, T, \vec{K}_B) G(\vec{R}, T) \tilde{R}_t(\omega) \end{aligned} \quad (25)$$

where  $\omega$  can be written as

$$\omega = 2k_r \frac{v_a}{R_0} \left[ x_0(1 - 2v_f/v_a) + X_{sh} - X + 2v_f T + \frac{u_x}{v_a} (X - v_a T) \right]. \quad (26)$$

The expression (25) is the general form for our model. It requires, as input, expressions for the Bragg wave spectrum,  $Sp$ , the tilt factor,  $G$ , the velocity shift,  $X_{sh}$ , and the advecting current,  $u_x$ , as functions of the long wave variables.

We note that when the Bragg coherence time,  $\tau_c$ , is much less than the look time interval, our result (25) is very similar to a multilook analysis in that it is an incoherent sum over average time,  $T$ , of signals coherent over a short (order  $\tau_c$ ) relative time  $\delta t$ . In this case, a single look SAR image will differ from a multi-look image only in the amount of speckle. Resolution would be limited by the correlation time, not the look time. Since our expression has averaged over the speckle, it is applicable to either single look or multilook if the time resolution function  $\text{Res}_t[\sqrt{2}(x_0 - v_a T)]$  is interpreted as a sum over looks of the resolution function for each look.

### 3. A Single Long Wave

To analyze expression (25) any further analytically, a form must be chosen for the  $\vec{R}$  and  $T$  dependence of the various quantities. A form which would be appropriate to situations such as the TOWARD experiment has only one long wave present, traveling with phase velocity  $\vec{v}_\phi$ . Then the time dependence of  $Sp, G, A, \sigma_k$  and  $\vec{u}$  can be eliminated by changing variables from  $\vec{R}$  to  $\vec{R}' = \vec{R} - \vec{v}_\phi T$ . This change of variables is often made; however we have only used it for the average variables,  $(\vec{R} + \vec{R}')/2$ , characteristic of the long waves and not for the difference variables,  $\vec{R} - \vec{R}'$ , which are dominated by the short waves and have a different time dependence; that characteristic of their own phase velocity,  $\omega_K/K$ .

An alternative change of variables, applicable only to a one-dimensional wave (no dependence on the coordinate parallel to the crest) is

$$Y' = Y$$

and

$$X' = X - \frac{v_\phi}{\cos\theta} T \quad (27)$$

where  $\theta$  is the angle between the wave velocity vector and the azimuthal direction. We present below the formula for either of these cases by letting  $\vec{R}' = \vec{R} - \vec{v}'_\phi T$  with  $\vec{v}'_\phi = \vec{v}_\phi$  for the first case mentioned and  $\vec{v}'_\phi = (v_\phi/\cos\theta, 0)$  for the one-dimensional case.

With the new variables  $\vec{R}'$  replacing  $\vec{R}$ , equation (25) becomes

$$\begin{aligned} \text{Image}(x_0, y_0) = & \int dX' dY' dT \text{Res}_y [ \sqrt{2} (Y' + v'_{\phi y} T - y_0) ] \text{Res}_x [ \sqrt{2} (X' + v'_{\phi x} T - v_a T) ] \\ & \text{Res}_t [ \sqrt{2} (x_0 - v_a T) ] Sp(\vec{R}', 0, \vec{K}_B) G(\vec{R}', 0) \bar{R}_t(\omega) \end{aligned} \quad (28)$$

with

$$\omega = \frac{2k_r v_a}{R_0} \left\{ x_0 \left[ 1 - \frac{2v_f}{v_a} \right] + X_{sh} - X' - (v'_{\phi x} - 2v_f) T + \frac{u_x}{v_a} [ X' + (v'_{\phi x} - v_a) T ] \right\} \quad (29)$$

Using Gaussian resolution functions it is now possible to carry out the  $T$  integral explicitly although the results are sufficiently messy that only the two special cases (1)  $v_{\phi y} = 0$  and (2)  $v_{\phi x} = 0$  will be shown below.

**Case 1.** One-dimensional long waves or azimuthally directed long wave patterns,  $v_{\phi y} = 0$ . In this case the  $Y'$  ( $= Y$ ) resolution is entirely controlled by the original  $y$  resolution function  $Res_y [\sqrt{2}(Y - y_0)]$ . On the other hand, the  $X'$  resolution is expected to be dominated by the result of the  $T$  integral.

Let us introduce a change of the variable from  $T$  to  $T'$  where

$$v_a T' = v_a T - x_0 \quad (30)$$

and define the SAR resolution  $\Delta x_0$  by

$$\Delta x_0 = \frac{R_0}{2k_r v_a \Delta T_s} \quad (31)$$

where the effective look time  $\Delta T_s$  is given by  $1/\Delta T_s^2 = 1/\Delta T^2 + 1/\tau_c^2$  and  $\Delta T$  is the nominal look time. In terms of these variables we obtain

$$\begin{aligned} \omega &= \frac{1}{\Delta x_0 \Delta T_s} \\ &\left[ x_0 \left( 1 - \frac{2v_f}{v_a} \right) + X_{sh} - X' \left( 1 - \frac{u_x}{v_a} \right) - \left( T' + \frac{x_0}{v_a} \right) \left( v_{\phi x} - 2v_f + u_x - \frac{v_{\phi x}}{v_a} u_x \right) \right] \\ \omega &\cong \frac{1}{\Delta x_0 \Delta T_s} [x'_0 + X_{sh} - X' - T'(v_{\phi x} + u_x - 2v_f)] \end{aligned} \quad (32)$$

neglecting terms of relative order  $u_x/v_a$  with  $x'_0 \equiv x_0(1 - v_{\phi x}/v_a)$ . The integral to be done is then

$$\begin{aligned} I &= \int \frac{dT'}{\sqrt{2\pi} \Delta T} \\ &\exp \left[ - \left\{ \frac{T'^2}{\Delta T^2} + \frac{[X' - x_0 - (v_a - v_{\phi x})T']^2}{\Delta x^2} + \frac{[x'_0 + X_{sh} - X' - T'(v_{\phi x} + u_x - 2v_f)]^2}{\Delta x_0^2} \right\} \right] \end{aligned} \quad (33)$$

where  $\Delta x$  is the width parameter in the Gaussian function

$$Res_x(x) = \frac{e^{-\frac{x^2}{2\Delta x^2}}}{\Delta x (2\pi)^{1/2}}$$

and  $v_a \Delta T$  is the corresponding parameter in  $Res_t(v_a t)$ , i.e.  $\Delta T$  is the look time. For the case where the beam width  $\Delta x$  is much larger than the distance covered in the integration time, i.e.,

$$\Delta x \gg v_a \Delta T \quad (34)$$

the second term in the exponent can be neglected and the result is

$$I = \frac{\exp \left[ \frac{-(x'_0 + X_{sh} - X')^2}{\Delta x_0^2 + (2v_f - v_{\phi x} - u_x)^2 \Delta T^2} \right]}{\left[ 1 + \frac{(-2v_f + v_{\phi x} + u_x)^2 \Delta T^2}{\Delta x_0^2} \right]^{1/2}} \quad (35)$$

The interpretation of this result is that the image is shifted from  $X'$  to  $X' - X_{sh}$  and is blurred by the intrinsic SAR resolution size  $\Delta x_0$  and the defocusing factor  $(-2v_f + v_{\phi x} + u_x) \Delta T$ . The defocusing can be removed by choosing

$$v_f = \frac{v_{\phi} + u_x}{2} \quad (36)$$

Comparing this to the formula (11) shows that the effective velocity is the average of the azimuthal components of the phase velocity of the large waves and the advective velocity of the small waves. Since, in practice,  $u_x$  is a function of which part of the long wave is being imaged and averages zero in the frame of the average current, the globally best setting corresponds to  $1/2$  the phase velocity of the long waves in that frame. This result has also been reported by Ivanov (1982, 1983), Ouchi (1983), and Rotherham (1983) whose models are similar to ours.

In the multi-look case (35) is changed only by being a sum over terms with  $x_0$  replaced by  $x_0 - (v_{\phi x} + u_x - 2v_f) T_n$  with  $T_n$  being the center time of the  $n^{th}$  look. Thus different looks will only be aligned if  $v_f = (v_{\phi x} + u_x)/2$  and will cause further defocusing otherwise.

The reason for this unexpected result is that there are two aspects of the defocusing of a SAR image by the velocity of the object. The first is the fact that the object being imaged has itself moved a distance  $v \Delta T$  during the time  $\Delta T$  it was being looked at. This blurring would occur in ordinary optical photography if several pictures were superimposed. The second aspect, unique to the coherence of the SAR picture process, is caused by the time-dependent velocity shift generated by the small, but time-changing, angle between the azimuthal velocity of the object and the necessarily rotating direction of the part of the radar beam which strikes it. The total change in this velocity shift in a time  $\Delta T$  is also  $v \Delta T$  giving a solid object a blurring distance of  $2v \Delta T$ . For the ocean surface, the long wave phase velocity is responsible for the motion of the object (the long wave) being imaged. However, the coherent phase changes responsible for the time-

dependent velocity shift are provided by the short waves. The total blurring distance is then  $v_{\phi x} \Delta T + u_x \Delta T$  which is the same as for a solid object moving at  $v = (v_{\phi x} + u_x)/2$ . In Appendices A, B and C we elaborate on this idea for simplified cases.

The defocusing effect on the energy spectrum of the long waves in the image is easily computed with the Gaussian resolution functions independent of the details of the modulation mechanism. In the expression (25) for the signal the  $T$  integral has been done (35) resulting in the convolution form

$$\text{Image}(x_0, y_0) = \int \frac{dX' dY'}{2\pi \Delta x_e \Delta y} e^{-\frac{(x'_0 - X'')^2}{\Delta x_e^2}} e^{-\frac{(y_0 - Y')^2}{\Delta y^2}} Sp(\vec{R}', 0, \vec{K}_B) G(\vec{R}', 0) \quad (37)$$

where  $X'' = X' - X_{sh}(X')$  is a nonlinear function of  $X'$  and  $\Delta x_e^2 = \Delta x_0^2 + (-2v_f + v_{\phi x} + u_x)^2 \Delta T^2$ . The dependence on focus setting, however, is entirely contained in  $\Delta x_e$  so the  $x_0$  Fourier transform of  $\text{Image}(x_0, y_0)$  can be easily carried out ( $u_x$  can be neglected for typical cases).

$$f(k_0, y_0) = e^{-k_0^2 \frac{\Delta x_e^2}{4}} \int e^{ik_0(X' - X_{sh})} Sp(\vec{R}', 0, \vec{K}_B) G(\vec{R}', 0) e^{-\frac{(y_0 - Y')^2}{\Delta y^2}} dX' dY'. \quad (38)$$

Thus, independent of the form of  $Sp$  and  $G$  and the velocity bunching mechanism in  $X_{sh}(X')$ , the focus setting dependence is given by

$$|f(k_0, \delta v)|^2 = C(k_0) \exp\left[-2k_0^2 \Delta T^2 (v_f - v_{\phi x}/2)^2\right] \quad (39)$$

Notice that the formula predicts the dependence on focus setting to depend only on well known parameters. In particular the shape of the curve does not depend on the correlation time  $\tau_c$ . Of course the normalization does depend on  $\tau_c$ , but we make no attempt to fit  $C(k_0)$ . Models that predict optimum focus settings also generally predict focus setting curves and it is a better test of the model to compare the entire curve with data. We will compare equation (39) with the experimental results in the TOWARD interim report [Shermdin et. al., (1986)]. The SAR look time in that experiment was 1.74 sec, so we choose  $\Delta T = 1.74 \text{ sec} / \sqrt{6} = 0.71 \text{ sec}$ , to give the same  $\langle t^2 \rangle$  as a square window of total width 1.74 sec. The waves analyzed had a 140m wavelength, so  $k_0 = 2\pi/140m$  and a

phase velocity  $v_{\phi x} = 15m/s$ . The airspeed was  $v_a = 225m/s$ . The comparison of equation (39) using these parameters and the experimental results is shown in Figure 2. The fit seems quite reasonable. The shape of the time window,  $Res_t(x_0 - v_a t)$ , has very little effect on the curve of Figure 2. For a square window of total width,  $\sqrt{6}\Delta T$ , the Gaussian function in (39) is replaced by  $sinc^2[k_0\sqrt{6}\Delta T(\delta v - v_{\phi x}/2)]$  which differs very little from (39) in the range plotted. The  $sinc^2$  factor is also obtained by Ouchi (1982). A detailed analysis of the TOWARD data is presented in the companion paper, [DeWitt et al., 1988].

Equation (39) shows that harmonics of the basic 140m wave will be much more sensitive to  $v_f$  [see also Ouchi (1983a)]. The magnitude of these harmonics at our optimum focus setting will also be reduced by the intrinsic SAR resolution through the  $\exp[-k_0^2 \Delta x_0^2/4]$  factor in (38). The simplest model of the relative size of the 70m signal induced by the velocity bunching mechanism has  $Sp$  and  $G$  as constants in which case the integral in (38) can be done and is proportional to  $J_n(nQ)$  where  $Q = k_1^2 v_{\phi} h_0 R_0 \cos \delta_0 / v_a$  and  $k_0 = nk_1$ . In this case the 70m signal should be  $\exp(-3k_1^2 \Delta x_0^2/4) [J_2(2Q)/J_1(Q)]^2 = 0.35$  smaller than the 140m signal, assuming a decorrelation time,  $\tau_c$ , of about 0.1sec as estimated in Appendix D. The data of Shemdin et al. (1986) shows a peak of about this size but it is found at a wavelength of 80 meters instead of 70 meters.

**Case 2.** Range directed long wave patterns,  $v_{\phi x} = 0$ . In this case the result of the  $T$  integral is to produce a narrow resolution along some band in the  $X' - Y'$  plane which is not necessarily perpendicular to the  $X'$ -axis as it was in case (1). The best resolution is again obtained by choosing the coefficient of  $T^2$  in the exponential to be as small as possible. Thus the best focus setting is  $v_f = 0$  as was expected since there are no velocities in the  $x$ -direction other than that of the airplane. With  $v_f = 0$  the resolution function is

$$\exp\left\{\frac{-[X' - x_0 - X_{sh}(Y')]^2}{\Delta x_0^2}\right\} \exp\left[\frac{-(Y' - y_0)^2}{\Delta y^2 + v_{\phi y}^2 \Delta T^2}\right] \quad (40)$$

showing the extra defocusing in the  $y$ -direction due to the motion of the scene and the velocity shift in the  $x$ -direction due to motion in the  $y$ -direction. In the multi-look case, expression (40) is replaced by a sum over looks with  $y_0$  replaced by  $y_0 - v_{\phi y} T_n$  where  $T_n$  is the time at the center of the  $n^{th}$  look. Thus successive looks will not be lined up and further blurring will occur unless successive looks are shifted by  $v_{\phi y} (T_{n+1} - T_n)$  in the  $y$ -direction before being added together.

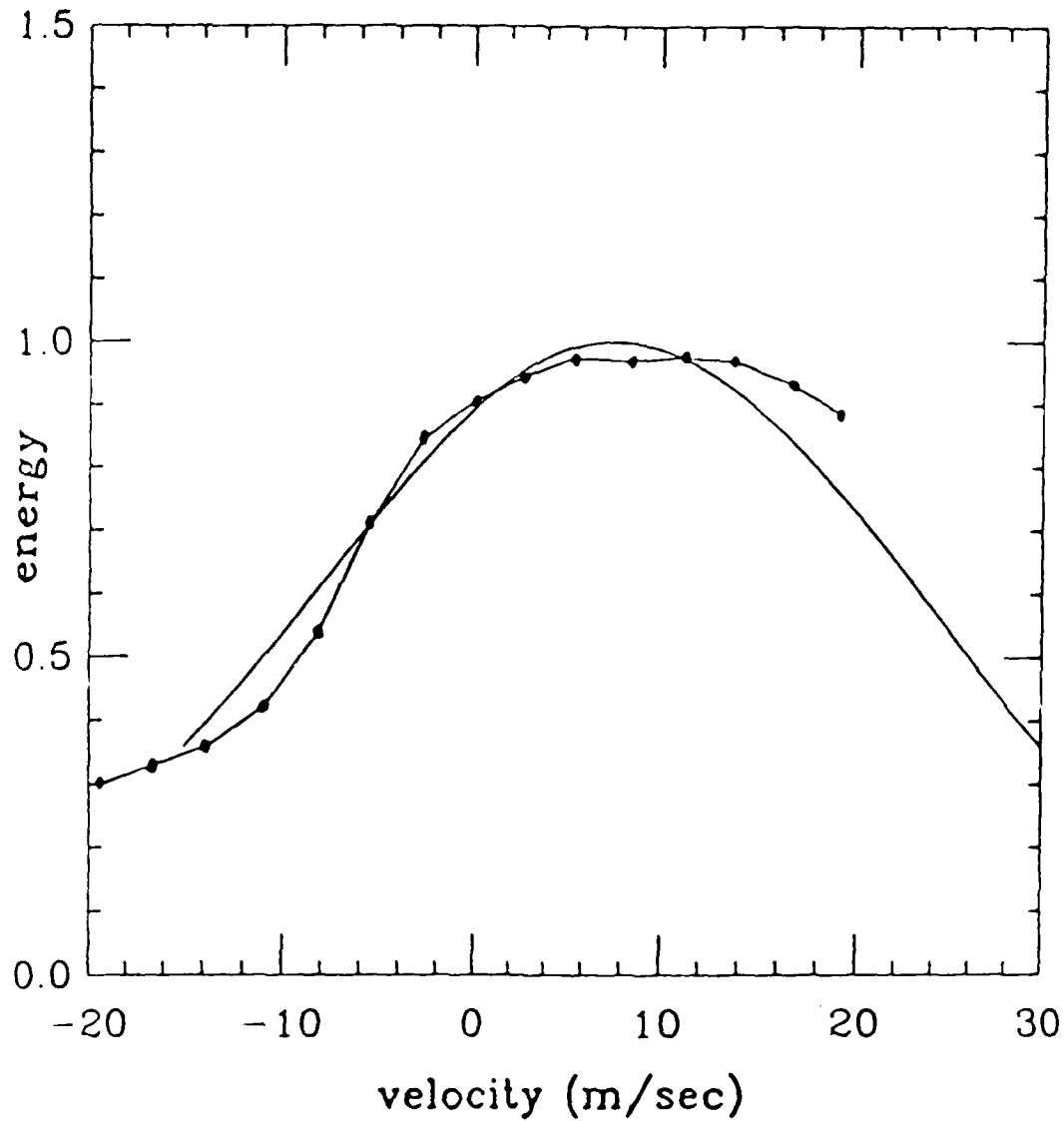


Figure 2. The energy at 140m in the spectrum of the image as a function of the focus setting of the SAR processor in units of the assumed velocity of the scene. The wave phase velocity is 15m/sec. The total look time is  $\sqrt{6}\Delta T = 1.74 \text{ sec}$ . The dots are the data from page VI-18 of Shemdin, et al. (1986) renormalized arbitrarily and the smooth curve is our expression (39).

The interpretation of this resolution function is easily seen by considering the case of a long narrow slick extending in a straight line in the range direction. The range-dependent velocity shift of the azimuthal image position would cause the image to have a sinusoidally-shaped slick ( $x_0 = \text{constant} \times \cos k_0 y_0$ ).

The resolution of this slick would be poorer in those regions where  $X_{sh}(Y')$  is changing most rapidly as a function of  $Y'$ . One could interpret this  $y_0$  variation of the resolution as a straightforward smearing in the  $x_0$  direction because of the averaging over  $Y'$ . Quantitatively

$$\Delta x_{eff}^2 \equiv \Delta x_0^2 + \left[ \frac{d X_{sh}}{d Y} \right]^2 (\Delta y^2 + v_\phi^2 \Delta T^2) \quad (41)$$

for the approximation  $X_{sh}(Y') = X_{sh}(y_0) + (Y' - y_0) d X_{sh}(y_0)/d Y$ . On the other hand, an alternative interpretation of this formula can be made in terms of coherence times.

The idea is that the long wave strains the Bragg wave and changes its wave vector. If the wave vector is changed enough to remove it from the Bragg resonance condition, coherence is lost. The condition that the wave vector has changed is that  $\Delta k \Delta y \sim \pi$ , where  $\Delta y$  is the resolution cell size in the  $y$  direction. In order to see the relationship between the two interpretations we substitute definitions (31) for  $\Delta X_0$  and (24) for  $X_{sh}$  to obtain

$$\Delta x_{eff}^2 = \left[ \frac{R_0}{2v_a k_r} \right]^2 \left[ \frac{1}{\Delta T_s^2} + \left[ 2k_r \frac{\partial u_{rad}}{\partial y} \right]^2 (\Delta y^2 + v_\phi^2 \Delta T^2) \right] \quad (42)$$

The second term in brackets will be reinterpreted to be the time  $\tau_s$  for the straining to occur. The straining of the Bragg wave by a current is given by

$$\frac{\partial \vec{k}}{\partial t} = -\vec{\nabla}(\vec{u} \cdot \vec{k}) = -k_B \frac{\partial u_y}{\partial y} = -2k_r \sin \delta_0 \frac{\partial u_y}{\partial y} = -2k_r \frac{\partial u_{rad}}{\partial y} \quad (43)$$

which for our geometry is

$$\frac{\Delta k_y}{\tau_s} \equiv \frac{\partial \vec{k}}{\partial t} = -k_B \frac{\partial u_y}{\partial y} = -2k_r \frac{\partial u_{rad}}{\partial y}, \quad (44)$$

and we will take  $\Delta k \approx \pi/\Delta y$ . The time  $\tau_s$  to strain the Bragg wave number out of resonance with the radar is thus given by

$$\frac{1}{\tau_s} \approx \frac{\Delta y \nabla \vec{u} \cdot \vec{k}_B}{\pi} \quad (45)$$

This strain is responsible for shortening of the effective coherence time and results in a broadening of the resolution,  $\Delta X_{eff}$ . Note that this formula has implicitly assumed that  $\vec{\nabla} \vec{u}$  is effectively constant over  $\Delta y$  so that it is only true for long waves. The more important decorrelation effect due to intermediate sized waves is discussed in Appendix D.

#### 4. Comparison with Other Models

In reviewing the literature to compare our model with other results we notice that the optimum focus setting results from a very subtle interplay between a number of small quantities, each of which may look negligibly small at various stages of the computation. Specifically, the frequency of the long wave is very small on the scale of the look time and the wavelength is very long on the scale of the resolution cell. However, the phase velocity of the long wave is the largest velocity on the ocean's surface and can easily be overlooked if thought of as frequency and wavelength.

In particular, when the coherence time is smaller than the look time it may be justified to neglect small frequencies when multiplied by coherence time but not justified to neglect these small frequencies when multiplied by the look time (i.e., in the incoherent sum). In Appendix D we make an estimate of the coherence time,  $\tau_c$ , and find values of about 0.1 sec for wind speeds of  $\sim 3m/sec$ . This is much smaller than the total look time for a multi-look SAR processor. Power series in  $\delta t$  are more justifiable than power series in  $T$ .

A second complication is that the best SAR image is not necessarily a good image of the small patches of the surface which do the scattering. The image of each patch of Bragg waves may be deliberately blurred in order to achieve a good image of the moving long wave. As an example of such a case we present in Appendix B a model of incoherent stationary scatterers whose radar reflectivity is modulated in time to correspond to a moving wave of reflectivity. The best focus for the wave is found for  $v_a (v_a - v_0) = (v_a - v_0/2)^2$  although the individual scatterers do not move at all. This model is also mentioned in Ivanov (1982). In the same spirit of sacrificing imaging of a patch of Bragg waves in favor of imaging the wave, we note that while the patch may be accelerating, and thus subject to blurring by way of a changing velocity shift, there is no acceleration defocusing of the image of the long wave (although there is acceleration defocusing of the image of any particular patch of Bragg waves) because at any given point on the long wave each patch moving past that point has the same velocity and thus a constant velocity shift.

Plant and Keller (1983) have proposed a method of simulating a SAR image by using data from a stationary two-scale radar wave probe. In their method the stationary radar probe data is analyzed on two time scales. Variations on the shorter time scale are used to measure the Doppler shift produced by surface motion while both this Doppler shift and the general intensity of the backscattered signal are functions of time on the longer time scale. Their procedure, like ours, assumes the auto-correlation time scale is short compared with the look time of the SAR system. They do not give explicit

formulae for the general focus setting case but only sketch the changes to be made. The primary change is to replace the frequency spectrum of the two-scale radar return signal  $f(\omega) = |\int e^{-i\omega t} E(t) dt|^2$  by the "chirped" frequency spectrum  $f(\omega, \Delta a) = |\int e^{-i\omega t - i\Delta a t^2} E(t) dt|^2$  with  $\Delta a = 2k_r v_a \Delta v / R_0 = 2k_r v_f v_a / R_0$ . The "chirping" is included because an object moving at the speed  $\Delta v$  would be expected to give a Doppler shift which would vary linearly in time because of the relative motion of the object and the SAR platform. The  $\Delta a$  term shows up in formulae (8) and (17) of Plant and Keller as an extra factor  $e^{i\Delta a (2t\tau + \tau^2)}$  inside the  $t$  and  $\tau$  integrals.

To determine the optimum value of  $\Delta a$  we must look at how the stationary data are used to generate a SAR simulation. Since the stationary probe makes measurements at one position  $x_p$  as a function of time  $t_p$ , while the SAR measurement uses information from many positions  $x$  as a function of time  $t$  the method of Plant and Keller assumes that only a few long waves are present so that stationary probe data at time  $t_p$  can be used at position  $x$  and time  $t$  such that  $x - v_\phi t = x_p - v_\phi t_p$ . When there is only *one* long wave present the time average (over the look time) in Equation 17 of Plant and Keller can be done by changing variables from  $x$  and  $t$  to  $x' = x - v_\phi t$  and  $t$  with the result that the only  $t$  dependence remaining is in the exponential factor

$$\exp[2i t \tau \Delta a] \exp\left[\frac{-2ik_r v_a v_\phi t \tau}{R_0}\right] \quad (46)$$

which is to be averaged over the look time. The largest value for the average is obtained by choosing  $\Delta a = k_r v_\phi v_a / R_0$  or equivalently by choosing the velocity shift  $\Delta v = v_\phi / 2$ . They did not discuss this point in their article.

Ouchi (1982, 1983a,b 1985) and Ivanov (1982) have constructed models of SAR imaging which are very similar to ours and also reach the conclusion that  $\Delta v = v_\phi / 2$ , consistent with our result  $\Delta v = (v_\phi + u_x) / 2$  when  $u_x$  is negligible. Our result has the pedagogical advantage that it gives consistent answers in all reference frames. Harger (1985) has also discussed the imaging of ocean waves. We briefly treat his model in Appendix C.

## 5. Direction Dependence of Image Contrast

The SAR image given by expression (37) contains contributions from velocity bunching, tilt modulation and hydrodynamic modulation. In this section we comment on the interaction of these effects and in particular on the sign of the velocity shift in the expression for  $X_{sh}$  [Equation (24)]. This shift is positive on the leading side of the wave crest and negative on the trailing side. For waves moving in the positive  $x$ -direction this tends to enhance the signal *interpreted* as coming from the troughs and diminish the signal from the crests. For waves moving in the negative  $x$ -direction (i.e., opposite to the airplane flight direction) the crests are enhanced and the troughs diminished. If the spectrum  $S_p(\vec{R}', 0, \vec{K}_B)$  is different in the trough than on the crests there would be an asymmetry in the visibility of the waves depending on the relative direction of the waves and the airplane. Although we have not yet made a model for the hydrodynamic modulation of the spectrum, we can choose the form

$$S_p(X', Y', 0, \vec{K}_B) G(X', Y', 0) = A (1 + b \cos k_0 x' + c \sin k_0 x') \quad (47)$$

and calculate the asymmetry by computing the integral in (38). Taking the long wave height as

$$h = h_0 \cos k_0 x' \quad (48)$$

the velocity shift is, from (24),

$$X_{sh}(x') = \pm \frac{R_0 \cos \delta_0}{v_a} k_0 v_\phi h_0 \sin k_0 x' \quad (49)$$

where  $\pm$  refer to the direction of propagation of the long wave relative to that of the airplane. The integrals in (38) can be done in terms of Bessel functions,  $J_m(Q)$ , with the result

$$f_{\pm}(k_0, y_0) = A' e^{-k_0^2 \frac{\Delta x_e^2}{4}} \left[ -J_1(\pm Q) + \frac{b}{2} (J_2(\pm Q) + J_0(\pm Q)) + \frac{c}{2i} (J_2(\pm Q) - J_0(\pm Q)) \right] \quad (50)$$

with  $Q = k_0^2 v_\phi h_0 R_0 \cos \delta_0 / v_a$  and the constant  $A'$  has absorbed several constant factors.

The asymmetry obtained by assuming equal values of  $\Delta x_e^2$  is

$$\frac{|f_+|^2 - |f_-|^2}{|f_+|^2 + |f_-|^2} = \frac{-2B}{1 + B^2 + C^2} \quad (51)$$

with  $B = b[J_2(Q) + J_0(Q)]/2J_1(Q)$  and  $C = c[J_2(Q) - J_0(Q)]/2J_1(Q)$ . The term  $c$  in (47) is out of phase with the other terms and thus diminishes the asymmetry so we set it equal to zero for the purpose of maximizing the asymmetry. In Figure 3 we plot the asymmetry given by (51) as a function of  $b$  for the case of long waves of wavelength 140m and peak-to-trough amplitude of 1.24m.

We also can try to use the tower based radar probe data of the University of Kansas group of the TOWARD experiment [Moore et al. (1986)] to predict the asymmetry expected for the TOWARD SAR data. This stationary probe measures the backscatter signal strength and the wave height (via the Doppler shift caused by the changing height). While the data show some sensitivity to radar frequency, look direction, and/or time of day, the most common situation has the strongest backscatter leading the crest by about  $90^\circ$  and the weakest backscattering trailing the crest by about  $45^\circ$ . If these numbers were both  $90^\circ$  we would have  $b = 0$  in expression (47) and there would be no asymmetry. Thus the sign of any asymmetry is sensitive to this phase. The data for the afternoon of October 31, 1984 show the phase of the radar power modulation transfer function to be somewhere between  $100^\circ$  and  $150^\circ$  at the peak of the wave height spectrum. A phase in this range favors the trough over the crest so a stronger image should be seen for waves moving in the same direction as the airplane. This is consistent with the preliminary analysis done on the SAR pictures for this date [Shemdin et al. (1986)]. Data for the afternoon of November 4, 1984 are not as complete but show the phase of the modulation transfer function may have been close to zero under the weather conditions prevailing then. A phase near zero would give stronger wave images for waves moving opposite to the direction of travel of the airplane. Analysis of SAR pictures for this date is incomplete [Shemdin et al. (1986)]. The size of the effect cannot be obtained from the Kansas Report [Moore et al. (1986)] which does not give the absolute normalizations for their results.

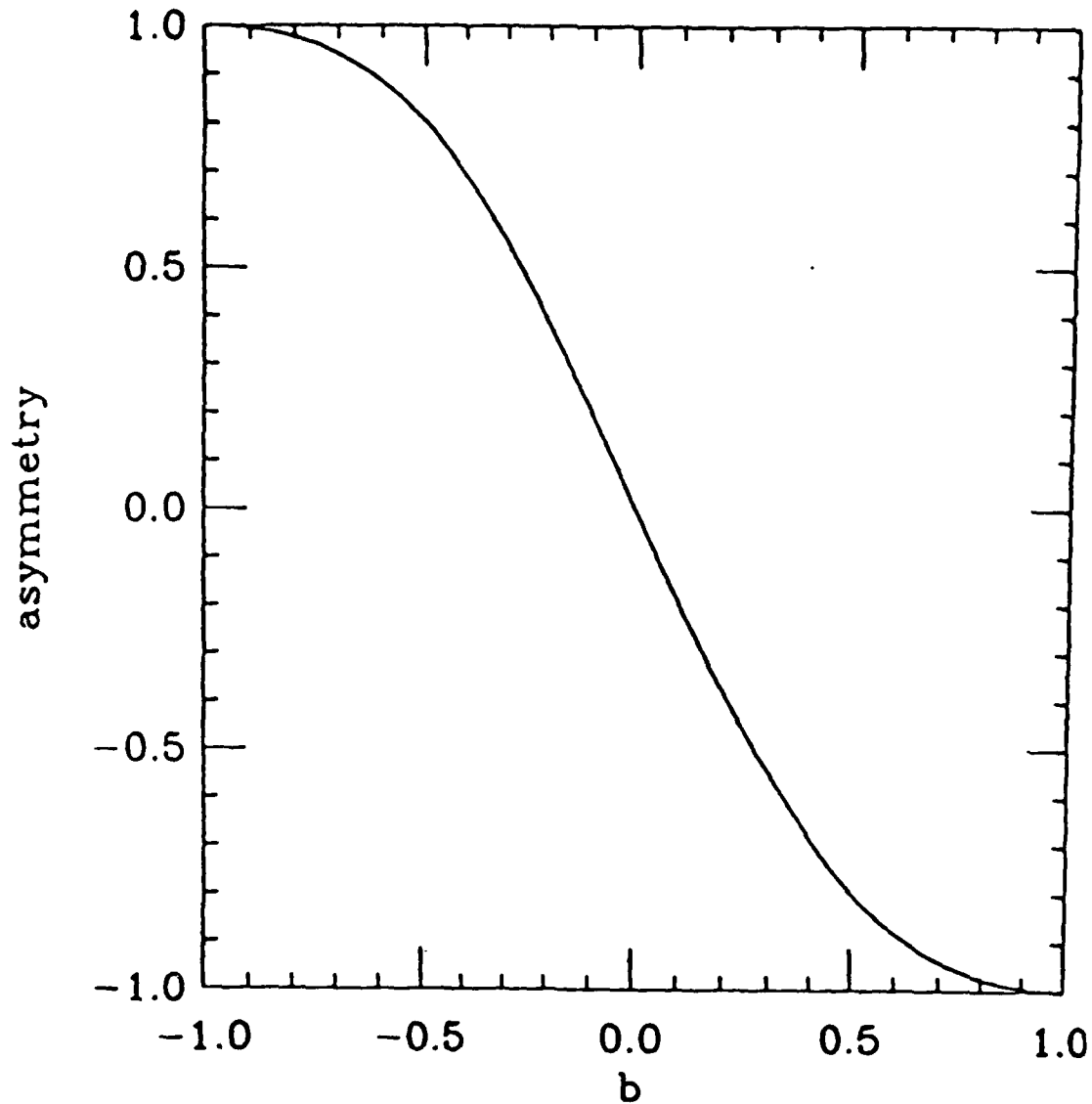


Figure 3. The asymmetry in the image's energy spectrum at best focus as a function of the amount of modulation in the radar reflectance. The asymmetry is defined as  $(|f^+|^2 - |f^-|^2) / (|f^+|^2 + |f^-|^2)$  where  $+$ ( $-$ ) refers to waves traveling in the same (opposite) direction as the airplane. The radar reflectance is parameterized as  $(1 + b \cos k_0 x)$ . The parameters for the velocity shift were taken to correspond to conditions in the TOWARD experiment.

## 6. Comments on Other Long Wave Patterns

We have already discussed in Section 3 an aspect of imaging which could be tested by imaging a long narrow slick in the presence of range directed waves. Such a slick could be laid down deliberately or one could use a natural slick or the turbulent wake of a range moving ship.

Another configuration which should be tested is that of the focus setting which best resolves the Kelvin wake of an azimuthally moving ship. In this case, the ship itself would prefer a focus setting  $\Delta v = v_{ship}$  since both the scatterer and the object to be imaged move at  $v_{ship}$ . On the other hand the wake would be best focused at  $\Delta v = v_{ship}/2$  since the scatterers (the Bragg waves) are slowly moving while the pattern to be imaged is moving at  $v_{ship}$ . Data for such a case may be present in SAR pictures already taken.

A particularly striking demonstration of this prediction would be to subtract images processed for two focus settings – one optimized for the waves and the other for the ship wake. By appropriately choosing the relative weighting, the waves could be made to nearly cancel (a smeared sine wave is a sine wave with a smaller amplitude). What would be left would be a sharply focussed ship wake surrounded by a negative image of the same wake smeared out.

For long waves at angle  $\phi$  with respect to the azimuthal direction, tests should be made of the prediction of Ouchi (1982)  $\Delta v = v_\phi / (2 \cos \phi)$ . This case should also be available in present data sets.

Finally we note that in the presence of several long waves there will be range acceleration defocusing of the image of one long wave by the other long waves passing through it - Bragg wave packets at a given phase along one long wave will not always have the same velocity shift because of the presence of the other long waves. We hope to explore numerically the effect of such degradation of images.

## Acknowledgement

This work was supported by ONR. We thank Omar Shemdin for several very useful discussions and for providing data on focus setting curves.

## Appendix A: An Example – “Windowed” Scatterers

We give an example of a system with a pattern velocity, showing how the focusing of SAR images depends on both pattern velocity and scatterer velocity. The purpose of this example is to attempt to understand our previously obtained result involving the focus setting. In Figure 4, the airplane is located at  $x_a = v_a t$ , while a “window” through which scatterers can be seen is at  $x_w = x_0 + v_w t$ , and the scatterers appear in the window moving with velocity  $v_s$ . The window represent a “pattern.”

The radar will see a given scatterer only for the short time it can appear in the “window” but because of the motion of the scatterer, the SAR processor will interpret the scatterer as being located at the velocity shifted position (neglecting the size of the window).

$$x_{image} = (x_0 + v_w t) - \frac{R}{v_a} v_{radial} \quad (A1)$$

The radial velocity of the scatterer depends on the relative location of the airplane and the window.

$$v_{radial} = -v_s \sin\theta \approx -v_s \frac{v_a t - (x_0 + v_w t)}{R} \quad (A2)$$

Substituting in the expression for  $v_{radial}$ , the image is at

$$\begin{aligned} x_{image} &= (x_0 + v_w t) (1 - v_s/v_a) + v_s t \\ &= x_0 (1 - v_s/v_a) + (v_s + v_w - v_s v_w/v_a) t \end{aligned}$$

Since this is a time dependent position it will be blurred by the motion unless it is reinterpreted as being focused behind the actual scene by a distance sufficient to give a stationary image as viewed from the airplane (see figure 4). Such a stationary point at  $x_1$  would satisfy

$$\frac{(v_a t - x_1)}{R_1} = \frac{v_a t - x_{image}}{R}$$

for all times. From the terms linear in  $t$  we get

$$\frac{v_a}{R_1} = \frac{v_a - v_s - v_w + v_s v_w/v_a}{R} = \frac{(v_a - v_w)(v_a - v_s)}{R v_a}$$

or

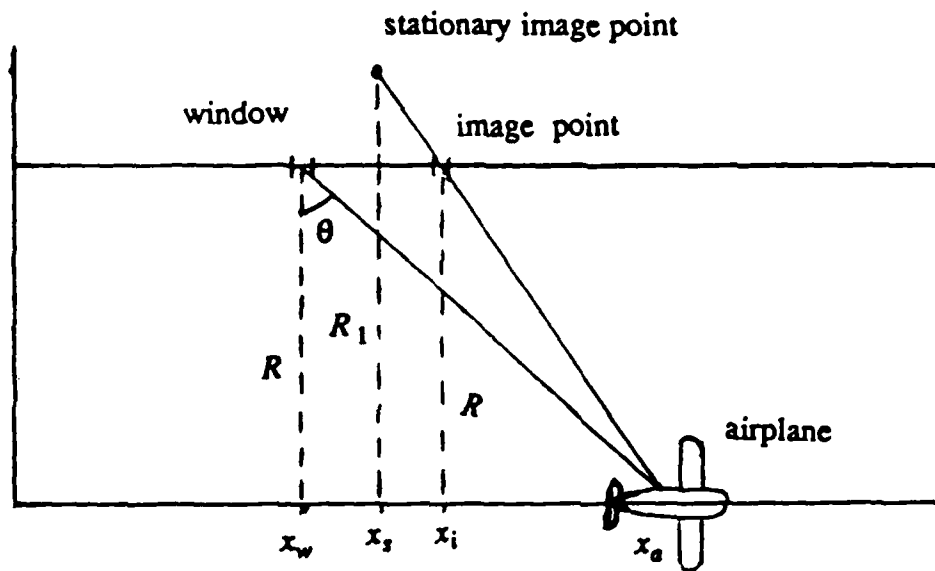


Figure 4. The SAR system on the airplane at  $x_a = v_a t$  picks up a signal from scatterers moving at speed  $v_s$  in the window at  $x_w = x_0 + v_w t$  and interprets them as coming from the velocity shifted image point  $x_i = x_w - (R/v_a)v_{radial}$  where  $v_{radial} = -v_s \sin\theta$ . This moving image point at range  $R$  can be reinterpreted as a stationary image point located at range  $R_1$  where

$$\frac{x_a - x_s}{R_1} = \frac{x_a - x_i}{R}$$

$$1 - \frac{2v_f}{v_a} = \frac{R}{R_1} = \frac{(v_a - v_w)(v_a - v_s)}{v_a^2} = 1 - \frac{(v_w + v_s)}{v_a}$$

For an ordinary object for which  $v_s = v_w = v$  this is the usual velocity focusing shift

$$\frac{R}{R_1} = 1 - \frac{2v}{v_a}$$

However, we see that it is really made up of 2 parts: one, the  $v_s$  Doppler shift effect, depends on the coherence of the scattering. The other, the  $v_w$  motion of the pattern to be imaged, is familiar to any photographer trying to point his camera to follow a moving object by lining up the incoherent images received at each instant by the camera.

The resolution of the window is governed by the incoherent addition of the images from each scattering appearing in the window for a time  $\tau = L/(v_s - v_w)$  where  $L$  is the size of the window. The SAR intrinsic resolution will be governed by the smaller of the time  $\tau$  and the look time  $T$ . If  $\tau$  is smaller than  $T$ , then any value of  $T$  will correspond to a multi-look SAR image.

The analogy to imaging of the ocean is readily apparent. The pattern velocity is the phase velocity of the long wave. The scatterer velocities are the sum of the Bragg phase velocity plus the advective velocity. The Bragg waves (at least for X band and probably for L band radar) lose their coherence in a time short compared to the usual SAR integration time. The window can be thought of as a particular part of the long wave.

This separation of effects also shows why there should be very little effect of acceleration in the imaging of a single long wave even though acceleration can be important for solid objects. The "pattern ('window') velocity which corresponds to the phase velocity of the long wave being imaged is constant for a single wave and nearly constant for a wave packet. The individual packet of small waves which actually does the coherent scattering is only viewed for a short time and so its velocity does not have time to change appreciably. Different scatterers might have different velocities as they appear in the window but since the "window" is to be taken to be a particular section of the long wave, the various Bragg waves appearing on this section should be quite similar since they are subject to the same advective currents.

## Appendix B: A wave of reflectivity in incoherent stationary scatterers

Consider the SAR signal from a collection of stationary scatterers for which the magnitude of the scattering depends on  $\cos(Kx - \Omega t)$ , where  $x$  is the position of the scatterer, but there is no corresponding space-time pattern for the phases. The phase of an individual scatterer is assumed to vary slowly with a decorrelation time  $\tau_c$ , and also to have no correlation with the phases of other scatterers. This model illustrates some of the features of scattering from the ocean surface where swell is present. There the intensity pattern moves with the phase velocity of the swell and the individual scatterers (Bragg waves) behave as independent scatterers with no phase correlation. The SAR image can then be obtained from the general expression (13) with  $A(x, y, t) = 0$  and

$$F(x, y, t) F^*(x', y', t') = \delta(x - x') \delta(y - y') F(KX - \Omega T - \Omega \delta t / 2) F^*(KX - \Omega T + \Omega \delta t / 2) \\ \approx \delta(\delta x) \delta(\delta y) |F(KX - \Omega T)|^2 e^{-\frac{(\delta t)^2}{4\tau_c^2}} \quad (B1)$$

for short correlation times,  $\tau_c$ . In this form, it is clear that a change of variables,  $X' = X - v_\phi T$ , without a corresponding change for the difference variable,  $\delta x$ , is appropriate and the  $T$  and  $\delta t$  integrals can be done explicitly as in Section 3 (Case 1), with the simplification that  $X_{sh} = 0$  and  $u_x = 0$ . In particular the  $T$  integral is

$$\int dT \text{Res}_x \left[ \sqrt{2}(X' - (V_a - V_\phi)T) \right] \text{Res}_t \left[ \sqrt{2}(x_o - V_a T) \right] \\ \exp \left\{ -2ik_r \frac{[(v_a \delta t)(X' - T(v_a - v_\phi)) + v_a^2 T \delta t (1 - 2v_f/v_a)]}{R_0} \right\} \quad (B2)$$

which is the Fourier transform of a Gaussian function of  $T$ . The largest value of this Fourier transform occurs for the transform variable

$$2k_r v_a \delta t \frac{[(v_a - v_\phi) - v_a(1 - 2v_f/v_a)]}{R_0} = 0, \quad (B3)$$

i.e. for  $v_f = v_\phi/2$ .

The conclusion is that in order to get a clear image of the moving pattern of reflectivity, sharp focusing of the stationary scatterers must be abandoned. Moreover, since the individual scatterers are not moving, there is no velocity shift due to their motion relative to the slightly "rotating" radar beam which scatters from them. Thus the image blurs only because of the motion of the pattern and not from motion of the scatterers. Thus the proper focus correction is  $v_f = v_\phi/2$ .

### Appendix C: The Effect of the Bandwidth of the Bragg Spectrum

Harger [1985] has considered the case of an ensemble of Bragg waves travelling entirely in the range direction, and obtained a optimal focus setting of  $v_\phi$ , instead of the  $v_0/2$  that we have obtained. In this appendix we show the relationship of his model with our calculations.

We begin by considering a single Bragg wave. To keep things simple, we imagine the big wave to be an azimuthally directed wave of reflectivity, and ignore  $A$ ,  $u$ , and  $\sigma$ . From the first of Eqs. 20, we see that there is a relation between  $K_x$  and  $x - v_a T$ , given by the beam rotation. Thus, instead of choosing a finite look time, we can nearly equivalently consider an infinite look time but a limited range of  $K_x$  values of the Bragg waves.

The radar return, integrated over  $y$  for a single  $x$  value is given by

$$R = C \exp \left[ \frac{i k_r (x - v_a t)^2}{R_0} + i K_x x \right] \left[ 1 + \frac{\alpha}{2} e^{i k_0 (x - v_\phi t)} + \frac{\alpha^*}{2} e^{-i k_0 (x - v_\phi t)} \right], \quad (C1)$$

where  $C$  is a complex amplitude. The first exponential is the radar phase, and the second is the  $x$ -dependent Bragg wave phase. The remaining factor gives the modulation by the big wave; we assume  $\alpha < 1$ , since it is proportional to the slope of the long wave in the real problem. We have ignored harmonics of  $k_0$ . The total return is, ignoring  $\text{Res}_x$ ,

$$\begin{aligned} \int R dx = C' & \left\{ \exp \left[ i K_x v_a t - \frac{i K_x^2 R_0}{4 k_r} \right] \right. \\ & + \frac{\alpha}{2} \exp \left[ i K_x v_a t + i k_0 (v_a t - v_\phi t) - \frac{i (K_x + k_0)^2 R_0}{4 k_r} \right] \\ & \left. + \frac{\alpha^*}{2} \exp \left[ i K_x v_a t - i k_0 (v_a t - v_\phi t) - \frac{i (K_x - k_0)^2 R_0}{4 k_r} \right] \right\}, \quad (C2) \end{aligned}$$

where uninteresting constants are lumped into  $C'$ . We now multiply by

$$\exp \left[ - (x_0 - v_a t)^2 \left[ \frac{i k_r}{R_0} (1 - v_f/v_a)^2 + \frac{1}{2 v_a^2 \Delta T^2} \right] \right] \quad (C3)$$

and integrate over time. The coefficient of  $(x_0 - v_a t)^2$  will appear as the complex width of a gaussian in  $K_x$ . The expression for the complex width can be simplified because, as is easily verified, the imaginary part is much larger than the real part provided that

$$\frac{1}{2\Delta T^2} < \frac{k_r v_a^2}{R_0}$$

We expand in the ratio of real to imaginary keeping only the first two terms. With this approximation we obtain the result for the amplitude of the signal assignment to the pixel located at  $x_0$  to be:

$$\begin{aligned} F(K_x, k_0, x_0) = C''(K_x) & \left\{ e^{iK_x x_0} e^{-\frac{i}{4} \frac{R_0}{k_r} \left[ K_x^2 - \frac{K_x^2}{(1 - v_f/v_a)^2} \right]} e^{-\frac{K_x^2}{2\Delta k^2}} \right. \\ & + \frac{\alpha}{2} e^{i \left[ K_x + k_0(1 - v_\phi/v_a) \right] x_0} e^{-\frac{i}{4} \frac{R_0}{k_r} \left[ (K_x + k_0)^2 - \frac{\left[ K_x + k_0(1 - v_\phi/v_a) \right]^2}{(1 - v_f/v_a)^2} \right]} e^{-\frac{(K_x + k_0(1 - v_\phi/v_a))^2}{2\Delta k^2}} \\ & \left. + \frac{\alpha^*}{2} e^{i \left[ K_x - k_0(1 - v_\phi/v_a) \right] x_0} e^{-\frac{i}{4} \frac{R_0}{k_r} \left[ (K_x - k_0)^2 - \frac{\left[ K_x - k_0(1 - v_\phi/v_a) \right]^2}{(1 - v_f/v_a)^2} \right]} e^{-\frac{(K_x - k_0(1 - v_\phi/v_a))^2}{2\Delta k^2}} \right\} \quad (C4) \end{aligned}$$

In this expression,  $\Delta k$  is given by,

$$\Delta k = \frac{2k_r v_a \Delta T}{R_0} .$$

This expression is complicated, but after some further manipulations the result will simplify. However it is worth pointing out the dependence on the focal setting velocity  $v_f$ . If one examines the term proportional to  $\alpha$ , it is evident that  $v_f$  appears in two places in the phase.

$$\text{These are } \frac{-R_0}{k_r} k_0 K_x \left[ 1 - \frac{(1 - v_\phi/v_a)}{(1 - v_f/v_a)^2} \right]$$

and

$$\frac{-R_0}{k_r} k_0^2 \left[ 1 - \frac{(1 - v_\phi/v_a)^2}{(1 - v_f/v_a)^2} \right] .$$

For small  $v_\phi/v_a$ , the first phase vanishes for  $v_f = v_\phi/2$ , and the second for  $v_f = v_\phi$ . Thus the proper focus setting will depend on which of the two phases is dominant.

As one can infer from the above equations, a range of  $K_x$ 's will contribute to the signal. The width of the range is given by  $\Delta k$ . In order to understand the origin of this width, we refer to equation 20 and the subsequent text. The rotation of the beam as the plane moves, leads to the above relationship between  $\Delta k$  and  $\Delta T$ . (Note: in the above derivation,  $\Delta k$  appeared naturally as a result of the  $t$  integration). In order to accommodate the signal from all Bragg waves, we integrate the signal return over  $K_x$ . The constant  $C(K_x)$  is proportional to the amplitude of the Bragg wave at wave number  $K_x$ . For future notational convenience we denote the integral over Bragg wave numbers by

$$amp(x_0) = \int dK_x F(K_x, k_0, x_0)$$

the next step is to take the Fourier transform of the intensity at the wave number  $k_0(1 - v_\phi/v_a)$ .

$$\begin{aligned} I(k_0) &= \int dx_0 e^{-i k_0 x_0 (1 - v_\phi/v_a)} |amp(x_0)|^2 \\ &= \int dx_0 e^{-i k_0 x_0 (1 - v_\phi/v_a)} \int dK_x \int dK'_x F(K_x, k_0, x_0) F^*(K'_x, k_0, x_0) \end{aligned} \quad (C5)$$

The only terms that contribute to this particular Fourier component will be linear in the modulation  $\alpha$ .

The next assumption is that Bragg waves with different  $K_x$  values have uncorrelated values of the complex factor  $C''(K_x)$ . In that case the only important (non-speckle) terms in the product  $FF^*$  are those which are diagonal in  $K_x$ . Since  $F$  is proportional to the Bragg wave amplitude, the product  $FF^*$  will be proportional to the Bragg wave spectrum  $Sp(K_x)$ . We now do the  $x_0$  integral to obtain the fourier transform of the intensity,

$$I(k_0) = const \int dK_x Sp(K_x) G(k_0, K_x, v_f)$$

where

$$\begin{aligned} G(k_0, K_x, v_f) &= \exp \left[ -\frac{K_x^2}{\Delta k^2} - \frac{k_0^2 (1 - 2v_\phi/v_a)}{2\Delta k^2} - \frac{iR_0}{2k_r} k_0 K_x (v_\phi/v_a - 2v_f/v_a) \right] \\ &\quad \cosh \left[ \frac{k_0 K_x}{\Delta k^2} \left( 1 - \frac{v_\phi}{v_a} \right) - \frac{iR_0}{2k_r} k_0^2 \left( \frac{v_\phi}{v_a} - \frac{v_f}{v_a} \right) \right] \end{aligned} \quad (C6)$$

and we have dropped quadratic terms in  $v_\phi/v_a$  and  $v_f/v_a$ .

Harger [1985] has considered the case of an ensemble of Bragg waves travelling in the range direction, i.e.  $k_x = 0$ . To obtain the result we can imagine that  $Sp(K_x)$  is a delta function at a particular  $K_x$ . Then we consider the absolute magnitude of  $G$ . The term involving  $v_\phi - 2v_f$  appears in phase and thus does not contribute to the magnitude. It is easy to verify that the maximum of the magnitude of  $G$  is obtained when  $v_\phi = v_f$ . However, normally there would be a spectrum of waves present and in fact the spectrum is expected to be relatively constant in the range

$$-\Delta k < K_x < \Delta k \quad .$$

In order to see the transition between a narrow spectrum and a broad spectrum we consider a form for  $Sp(K_x)$  such that the transition can be easily seen.

$$Sp(K_x) = \text{const } e^{-(K_x - k_c)^2 / 2\mu^2} \quad .$$

with this form the spectrum, the integral over  $K_x$  can now be done. For simplicity let  $k_c = 0$ . Then

$$I(k_0) = \cos \left[ \frac{R_0 k_0^2}{2k_r} (v_f/v_a - v_\phi/v_a) + \frac{\mu^2}{(\Delta k^2 + \mu^2)} (v_\phi/v_a - 2v_f/v_a) \right] \exp \left[ - \frac{R_0^2 k_0^2 (v_\phi/v_a - 2v_f/v_a)^2 \Delta k^2 \mu^2}{16 k_r (\Delta k^2 + \mu^2)} \right] \quad (C7)$$

As discussed above, the part dependent on  $\frac{R_0}{k_r} k_0^2$  has  $v_f - v_\phi$ , while the part involving  $k_x$ , which has become the part involving  $\mu$  on integration, has  $v_\phi - 2v_f$ .

For typical SAR parameters the argument of the cosine is very small. Consider first the case of a narrow spectrum, then  $\mu^2 \rightarrow 0$  and the maximum of  $I(k_0)$  is obtained when  $v_f = v_\phi$ . Note however that this is a very flat maximum and the focus setting makes very little difference. This corresponds to the case Harger [1985] analyzed.

Next consider the case of  $\mu \rightarrow \infty$  which means the spectrum does not vary much. Then the second term in the cosine is much larger than the first and  $v_f = v_\phi/2$  maximizes the cosine term. The exponential is maximum when  $v_f = v_\phi/2$  as well. The maximum of the exponential is much sharper.

The conclusion is that as long as the spectrum is reasonably flat over the region  $-\Delta k < K_x < \Delta k$ , the proper focus setting is  $v_\phi/2$ . If the spectrum of Bragg waves is sufficiently narrow the proper setting is  $v_\phi$ ; however, the actual focus setting does not matter much in the latter case.

#### Appendix D: Decorrelation time for SAR reflections from Bragg Waves.

The waves intermediate in wavelength between the Bragg waves and the waves being imaged cause a degradation of resolution. There are alternative interpretations of the reason for the degradation that lead to the same final expression. It is important to emphasize that the following discussion refers to the same mechanism, but different interpretations.

One way of understanding image degradation is to consider the random position shifts due to the orbital velocities of the intermediate waves which are typically traveling in many different directions. This gives a blurring of the image. Another way of understanding the same phenomena is to consider the phase coherence time of Bragg waves. By phase coherence time we mean the time it takes for different patches of Bragg waves to change their relative phases significantly. Phase coherence of the scatterers is necessary since phase information is used to infer position. The patches of Bragg waves in different locations are advected by currents due to the orbital velocities of the intermediate waves. These currents Doppler shift the frequencies of the Bragg waves and since the currents have a random character, the phases of all the Bragg waves will evolve differently, leading to incoherence and image degradation. This appendix will derive an expression for the degradation.

In Eq. (18) a function  $D(t)$  was introduced that contained a decorrelation time for Bragg waves due to damping, wind and modulation by intermediate size waves. It was perhaps premature to introduce the part relating to modulation by intermediate size waves. If we proceed to Eq. (23) and extract the terms linear in the intermediate wave variables and ignore the last term we have to consider the expression

$$\exp \left[ 2i k_r [\sin \delta_0 u_y (\vec{r}, T) - \cos \delta_0 u_z (\vec{r}, T)] \delta t \right] . \quad (D1)$$

This phase can be seen in Equations (22)-(24) of the main text, where we were thinking specifically of the long waves and could replace  $\vec{r}$  by  $\vec{R}$ . For the intermediate waves we can treat  $\vec{u}$  as a randomizing influence on the phase of the signal. Taking an ensemble average over these intermediate wave advection currents and assuming they are Gaussian random variables yields an explicit form for the decorrelation function  $D(\delta t)$  introduced in Equation (18).

$$\begin{aligned} D(\delta t) &= \langle \exp [ 2i k_r (\sin \delta_0 u_y - \cos \delta_0 u_z) \delta t ] \rangle \\ &= \exp \left[ - \langle \sin^2 \delta_0 u_y^2 + \cos^2 \delta_0 u_z^2 \rangle \frac{(2k_r \delta t)^2}{2} \right] . \quad (D2) \end{aligned}$$

The correlation time,  $\tau_c$ , can be read off as

$$\tau_c^{-1} = \sqrt{2} (2k_r) \left[ \sin^2 \delta_0 \langle u_y^2 \rangle + \cos^2 \delta_0 \langle u_z^2 \rangle \right]^{1/2} . \quad (D3)$$

This result is similar to that of Alpers et al. as reported in Shemdin et al. (1986).

Evaluation of  $\langle u_j^2 \rangle$  using several forms of the wave spectrum indicates the spectrum shape is not critical. The simplest to evaluate uses a wave height spectrum

$$s(\vec{q}) d^2 \vec{q} = \left[ B f(\alpha) / q^4 \right] d^2 \vec{q} \quad (D4)$$

with  $B = 2 \times 10^{-3}$  and  $\int_0^{2\pi} f(\alpha) d\alpha = 1$  where  $\alpha$  is the angle of  $\vec{q}$ . Then, for example,

$$\begin{aligned} \langle u_z^2 \rangle &= \int (gq) \left[ B f(\alpha) / q^4 \right] q dq d\alpha \\ &= Bg \int_{q_{\min}}^{q_{\max}} dq / q^2 . \end{aligned} \quad (D5)$$

The integral in (D5) is insensitive to the upper limit and choosing  $q_{\min} = g/v_w^2$ , where  $v_w$  is the wind speed, produces

$$\langle u_z^2 \rangle = B v_w^2 \quad (D6)$$

The range advection term  $\langle u_y^2 \rangle$  depends on the wind direction but is generally a little smaller than  $\langle u_z^2 \rangle$ . A reasonable estimate of  $\tau_c$  is then

$$\tau_c^{-1} = \sqrt{2} (2k_r) \sqrt{B} v_w = v_w / (0.3m) . \quad (D7)$$

For a 3m/sec wind speed,  $\tau_c = 0.1$  sec. We have tried other shapes and get  $\tau_c$ 's within the range 0.05-0.15 sec for TOWARD conditions.

At higher wind speeds the cutoff wavelength we have used,  $\lambda_{cm} = 2\pi v_w^2 / g$ , becomes longer than the pixel size and one might think that the velocity shift from the advection should no longer be treated as a randomizing influence on the phase of the signal from one pixel, but rather as an actual velocity shift for that pixel. That is correct for the position space image. On the other hand, the velocity shift of individual pixels by the intermediate waves can again be thought of as a randomizing process on the phase of the long wave signal, e.g. it is random from one crest of the long wave to the next. Averaging over this randomizing effect on the shift,  $X_{sh}$ , in Equation (38) leads to an expression which is equivalent to that obtained by including all intermediate waves independent of pixel size, in the expression for  $\tau_c$ . Thus as far as the long wave spectrum is concerned, it is unnecessary to divide the advection effects into decorrelation by the shorter intermediate waves and velocity shifting by the longer intermediate waves. Both effects contribute in the same way, thereby avoiding the necessity of deciding where to put the

dividing line between them. They are really the same mechanism with a different interpretation.

### References

- Alpers, W., and C. L. Rufenach, The effect of orbital motions on synthetic aperture radar imagery of ocean waves *IEEE Trans. Antennas Propag.*, AP-27, 685-690, 1979.
- DeWitt, R.J., Henyey, F.S. and Wright, J.A., "Comparison of Computed SAR Focus-Setting Curves with Model Predictions," La Jolla Institute, LJI-88-P-484.
- Harger, R., "The SAR image of short gravity waves on a long gravity wave" in Wave Dynamics and Radio Probing of the Ocean Surface, O. M. Phillips and K. Hasselmann, eds. New York: Plenum (1986) pp. 371-392.
- Henyey, F.S., Creamer, D.B., Dysthe, K.B., Schult, R.L. and Wright, J.A., "The energy and action of small waves riding on large waves," *J. Fluid Mech.* **189**, pp. 443-462, 1988.
- Ivanov, A. V., On the synthetic aperture radar imaging of ocean surface waves, *IEEE J. Ocean Eng.*, OE-7, 96-103, 1982.
- Ivanov, A. V., On the mechanism for imaging ocean waves by synthetic aperture radar, *IEEE Trans. Antennas Propag.*, AP-31, 538-541, 1983.
- Jain, A., Focusing effects in synthetic aperture radar imaging of ocean waves, *Appl. Phys.*, **15**, 323-333, 1978.
- Jain, A., SAR imaging of ocean waves: Theory, *IEEE J. Ocean Eng.*, OE-6, 130-139, 1981.
- Jain, A., and O. H. Shemdin, L band SAR ocean wave observations during MARSEN, *J. Geophys. Res.*, **88**, 9792-9808, 1983.
- Moore, R. K., A. Chaudhry, R. Lawner, J. Nice, and J. Boberg, The University of Kansas radar backscatter measurements from the ocean surface during the TOWARD 84/85 experiment, Radar Systems and Remote Sensing Laboratory Technical Report RSL TR 419-4, November 1986.
- Ouchi, K., Imagery of ocean waves by synthetic aperture radar, *Appl. Phys.* B-29, 1-11, 1982.
- Ouchi, K., Defocus dependence on ocean wave shape in synthetic aperture radar imagery, *Opt. Quantum Electron.*, **15**, 355-357, 1983a.
- Ouchi, K., Effect of defocussing on the images of ocean waves, in *Satellite Microwave Remote Sensing*, edited by T. D. Allan, pp. 209-222, Ellis Horwood, Chichester, England, 1983b.

- Ouchi, K., On the multilook images of moving targets by synthetic aperture radars, *IEEE Trans. Antennas Propag.*, AP-33, 823-827, 1985.
- Phillips, O. M., *The Dynamics of the Upper Ocean*, Cambridge University Press, 1977.
- Plant, W. J. and W. C. Keller, The two-scale radar wave probe and SAR imagery of the ocean, *J. Geophys. Res.*, 88, 9776-9784, 1983.
- Rotheram, S., Theory of SAR ocean wave imaging, in *Satellite Microwave Remote Sensing*, edited by T. D. Allan, pp. 155-186, Ellis Horwood, Chichester, England, 1983.
- Shemdin, O. H., Investigation of physics of synthetic aperture radar in ocean remote sensing, TOWARD 84/86 field experiment, Interim report, May 1986.